nature communications

Article

https://doi.org/10.1038/s41467-026-70081-3

Strong nickel enrichment co-located with redox-organic interactions in Neretva Vallis, Mars

Received: 17 November 2025

Accepted: 5 February 2026

Published online: 31 March 2026

Check for updates

H. T. Manelski[1] ✉, R. C. Wiens[1], A. Broz[1], J. A. Hurowitz[2], M. Tice[3], S. Clegg[4], E. Dehouck[5], N. Randazzo[6], S. A. Connell[1], O. Forni[7], S. J. VanBommel[8], S. Schröder[9], L. Mandon[10], T. S. J. Gabriel[11], C. C. Bedford[1], R. K. Martinez[4], E. A. Cloutis[12], A. Cousin[7] & M. L. Cable[13]

In 2024, NASA's Perseverance rover explored Neretva Vallis, an ancient river channel that once transported water into Jezero crater. There, the rover encountered Mg-poor mudstones with diverse alteration features. In 32 rock targets in Neretva Vallis, nickel (Ni) was detected by the SuperCam instrument with concentrations in individual rocks as high as ~1.1 weight percent – the highest abundance ever seen in bedrock on Mars. In this work, we describe and contextualize these Ni enrichments using outcrop-scale imagery and petrographic-scale elemental maps provided by the PIXL instrument. We find Ni enrichment in Fe-sulfides and their weathering products. The geochemistry and morphology of Neretva Vallis Fe-sulfides are similar to pyrite present in terrestrial Archean and Paleoproterozoic sedimentary rocks. As an essential element for terrestrial microbial life, the proximity of Ni enrichments to reduced sulfur and organic matter adds to the interest in bringing back to Earth the rock sample collected by Perseverance at this location, which could provide key insights into complex redox chemistry on early Mars.

The Mars 2020 Perseverance rover landed in Jezero crater, Mars, in February 2021 with the goal of searching for ancient habitable environments and collecting cored samples for eventual return to Earth as part of a future Mars Sample Return mission[1]. Jezero is a 45 km-diameter Noachian (~3.8–4.0 Ga) impact crater that once hosted a lake, as evidenced by two inlet valleys, their associated fluvio-deltaic fans, and an outlet valley on the eastern edge of the crater[2]. Since landing, the rover has traversed the igneous crater floor[3,4], ascended onto the western fan deposit[5], crossed the olivine- and carbonate-rich Margin Unit (MU)[6], and entered into the western inlet valley known as Neretva Vallis.

Investigation of Neretva Vallis began to the north, where Perseverance discovered a light-toned bedrock exposure named Bright Angel (BA) (Fig. 1c). Here, the rover identified clay-bearing mudstones overprinted by diagenetic features such as nodules and mineral veins[7]. At BA the rover also found 'leopard spots': mm- to sub-mm scale rounded reaction fronts with cores of Fe-sulfide, alongside detections of organic carbon[7]. South of BA lies the Masonic Temple (MT) exposure, where outcrops exhibit similar expressions but also contain poorly sorted, unstratified conglomerates with diverse, mm- to cm-scale clasts, including highly oxidized clasts of mudstone. These lithologies within Neretva Vallis collectively comprise the BA formation.

The features and textures of the BA formation indicate deposition in a low-energy, likely lacustrine, environment and while the structure

[1]Purdue University, West Lafayette, IN, USA. [2]Stony Brook University, Stony Brook, NY, USA. [3]Texas A&M University, College Station, TX, USA. [4]LANL, Los Alamos, NM, USA. [5]Université Claude Bernard Lyon 1, ENS de Lyon, CNRS, Villeurbanne cedex, France. [6]University of Alberta, Edmonton, AB, Canada. [7]IRAP, Toulouse, France. [8]Washington University, St. Louis, MO, USA. [9]DLR Institute of Space Research, Berlin, Germany. [10]Institut de Planétologie et d'Astrophysique de Grenoble, Grenoble, France. [11]USGS, Flagstaff, AZ, USA. [12]University of Winnipeg, Winnipeg, MB, Canada. [13]NASA Jet Propulsion Laboratory, Pasadena, CA, USA. ✉e-mail: hmanelsk@purdue.edu

https://doi.org/10.1038/s41467-026-70081-3

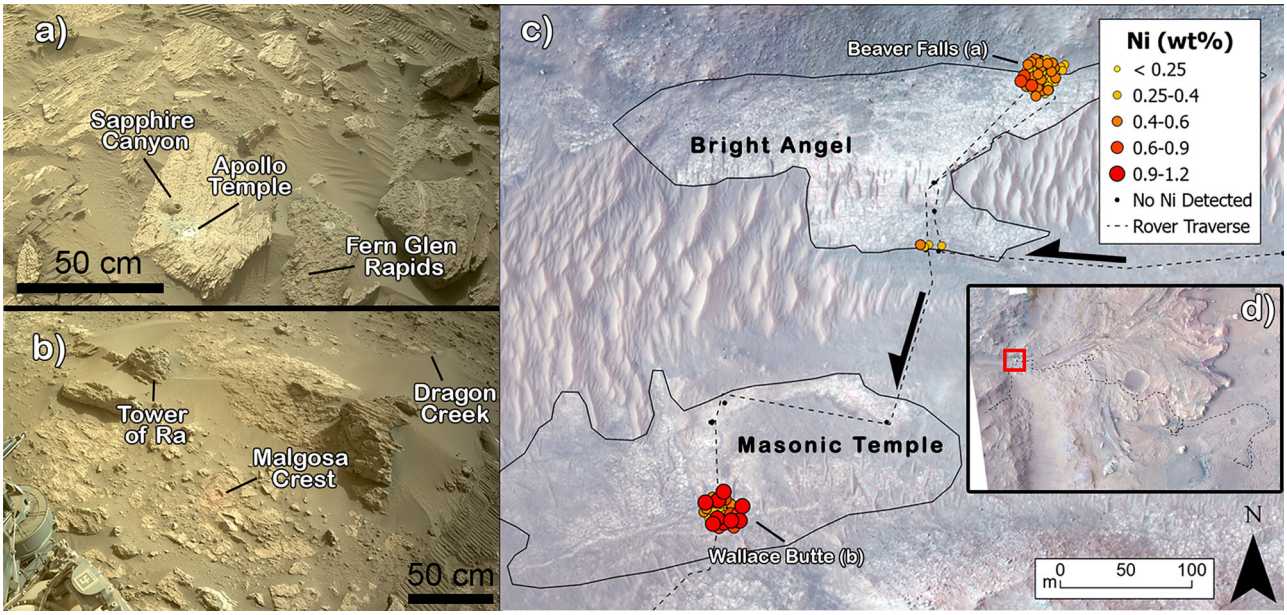

Fig. 1 | Magnitude and distribution of Ni discovered by SuperCam in Jezero Crater, Mars. Perseverance rover Navcam images of the Beaver Falls (**a**) and Wallace Butte (**b**) workspaces. The sample borehole (Sapphire Canyon), PIXL scans (Apollo Temple and Malgosa Crest), and rocks with major Ni-enrichments detected by SuperCam (Apollo Temple, Fern Glen Rapids, Dragon Creek, and Tower of Ra) are labelled. **c** Nickel detections with SuperCam in Neretva Vallis, showing the locations of the Bright Angel and Masonic Temple outcrops (points offset for clarity). Half arrows indicate the direction of travel of Perseverance. **d** Context HiRISE composite image of Jezero crater with red box to indicate the extent of panel (**c**). Image Credit: NASA/JPL-Caltech.

of the unit may support that it is a younger deposit, the age relationship to the MU exposed in the channel walls remains poorly constrained[7]. As such, these rocks may represent a young, channel-fill deposit, or a much older unit exposed by the incision of Neretva Vallis[8]. Geochemically, BA formation rocks are distinct from rocks encountered elsewhere in Jezero crater – including in the MU, western fan, crater floor, and Jezero watershed materials inferred from orbital remote sensing[9,10]. The BA formation is exceptionally Mg-poor (averaging ~2 wt% MgO) and contains higher abundances of SiO_2, Al_2O_3, and FeO_T relative to the mafic-ultramafic rocks investigated elsewhere in Jezero crater. This pronounced geochemical difference suggests a unique provenance or paleoweathering history.

Results

Ni enrichments discovered by SuperCam LIBS

Throughout rock exposures in Neretva Vallis, enrichments in nickel (Ni) were detected by the SuperCam instrument via the remote Laser Induced Breakdown Spectroscopy (LIBS) technique. This marked the first detection of Ni with SuperCam, apart from an enigmatic class of highly altered Al-rich float rocks found scattered across the Perseverance rover's traverse[11]. SuperCam is a mast-mounted instrument with a suite of remote spectroscopic techniques including LIBS, visible/near-infrared (VISIR), and Raman spectroscopy[12,13]. LIBS samples spots of ~100–450 μm in diameter, meaning most observations sample a mixture of minerals when grain size is smaller than the LIBS footprint[14]. This is particularly true of Neretva Vallis sedimentary rocks, which have a grain size of ~40–60 μm according to X-ray diffraction[7]. SuperCam LIBS observations are arranged in rasters and are sensitive to various major and trace elements including Ni[13,15]. SuperCam's Ni calibration model has a limit of detection of ~0.12 wt. % and a root mean squared error of prediction (RMSEP) of 0.12 wt. % (see Methods for more details). Ni was detected (>0.12 wt. %) in 32 of the 126 distinct rock targets analyzed by SuperCam LIBS in Neretva Vallis (Fig. 1). These Ni-rich targets are concentrated in two distinct localities: Beaver Falls and Wallace Butte (Fig. 1).

In northern Neretva Vallis (the Beaver Falls workspace, Figs. 1a, c, and 2), Ni is observed to be elevated in targets located within ~5 meters of both sides of the contact between the MU and BA sedimentary rocks. Detections of Ni are found within the dominant mudstone/siltstone lithology of BA at this location (e.g., Apollo Temple abrasion, Fig. 1a and "Soap Creek", Fig. 2). Concentrations of 0.19–0.24 wt. % Ni were found in the most Fe-rich points of each SuperCam raster – suggesting it is present in a Fe-rich phase (Supplementary Data 1). Ni was also detected in a series of Ca-sulfate veins (e.g., Seiber Point, Fig. 2) which cross-cuts the primary mudstone lithology. In these veins (4 distinct SuperCam targets), 0.33–0.56 wt. % Ni was observed (Supplementary Data 1), but only in visibly dark Fe-rich points – suggesting Ni is present in a Fe-rich phase mixed with Ca-sulfates. SuperCam also detected up to 0.83 wt.% Ni (Supplementary Data 1) across the contact in the adjacent olivine-rich MU to the north as well as the Fern Glen Rapids member (Fig. 1a), a moderately sorted granule conglomerate interpreted as a subaqueous debris flow with clasts potentially derived from the MU. Notably, Ni-rich rocks in the putative MU exhibit high Fe and S abundances with LIBS, suggesting the presence of Fe-sulfide or Fe-sulfate.

Following the exploration of the BA-MU contact, Perseverance drove south into MT (Fig. 1c), a bedrock exposure near the southern wall of the Neretva Vallis channel. First observed there were the poorly sorted and highly oxidized conglomerates of the Mount Spoonhead workspace, where no significant Ni concentrations were detected. A traverse further south revealed the Wallace Butte workspace (Figs. 1b, c), characterized by a highly-oxidized (red) flat-lying conglomerate facies, with abundant mudstone matrix (e.g., Dragon Creek and Wallace Butte, Fig. 1b) as well as higher standing, dark, Fe-rich rocks (e.g., Tower of Ra, Fig. 1b) – both of which had strong Ni detections with SuperCam. Ni enrichments in the bulk mudstone (eight distinct observations) ranged from 0.14–1.21 wt. % (Supplementary Data 1) - with the highest values seen in Fe-rich LIBS observations, again indicating the presence of Ni in a Fe-bearing phase.

https://doi.org/10.1038/s41467-026-70081-3

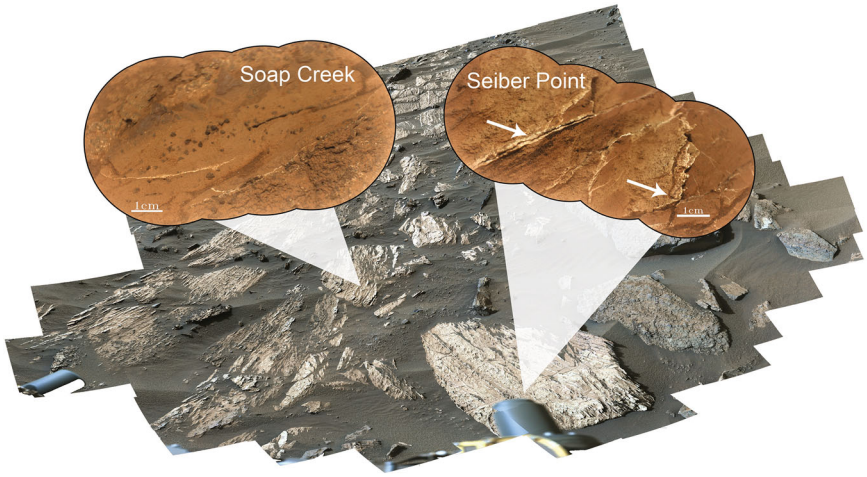

Fig. 2 | In Beaver Falls, Ni was detected in both the primary mudstone and within cross-cutting Ca-sulfate veins. Perseverance rover Mastcam-Z mosaic of the Beaver Falls workspace. Transparent polygons indicate the position of two SuperCam observations where Ni was detected in the dominant mudstone lithology (Soap Creek) and in Ca-sulfate veins (Seiber Point). The Ca-sulfate veins in Seiber Point are highlighted with white arrows. Soap Creek had three points with Ni quantified from 0.38–0.44 wt.%. In Seiber Point, three points were observed with 0.24–0.53 wt.% Ni. SHERLOC and PIXL scans which discovered locally reduced sulfur and organic matter were located on the light-toned rock that the Seiber Point sulfate veins cross-cut. Image Credit: NASA/JPL-Caltech/MSSS.

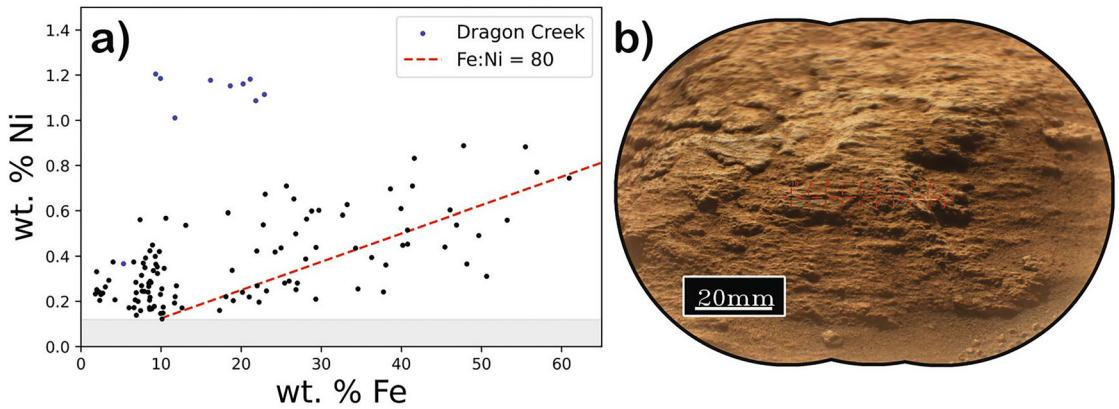

Fig. 3 | Ni vs Fe weight percent for SuperCam Targets in Neretva Vallis. a Weight percent Ni vs Fe for all detections of Ni with SuperCam LIBS in Neretva Vallis. The highest Ni concentration observed ("Dragon Creek") is shown in a SuperCam Remote Micro Imager context image (**b**) with red crosshairs marking the position of LIBS analyses. In grey (**a**) is below the limit of detection of Ni with SuperCam. Image Credit: NASA/JPL-Caltech.

It is unclear whether the higher standing Ni-rich rocks (0.39–0.88 wt. %, Supplementary Data 1), are float rocks or, instead, represent poorly exposed and weathered bedrock. Notably, SuperCam infrared spectra (co-located with LIBS) of the Tower of Ra and Elaine Castle targets (Fig. 1b) exhibit a weak absorption band at 2.27 μm and weaker features near 2.42, 2.46, and 2.53 μm (Fig. S1) – consistent with jarosite[16,17]. A nearby high standing Fe-rich float rock, Phantom Creek, exhibits a strong spectral signature of the chlorine bearing iron oxide akaganeite but shows no Ni detection with SuperCam LIBS[16,18].

Ni detections with SuperCam LIBS are highly localized within Neretva Vallis and have not been observed in bedrock targets elsewhere in Jezero Crater. In the dominant mudstone lithology of Beaver Falls, less than half of individual LIBS observations show elevated Ni detections (>0.12 wt. %), which suggests Ni is present in a minor, possibly dispersed, host phase. In contrast, within the Fern Glen Rapids facies, Ni abundances are consistently elevated across LIBS rasters, indicating either enhanced concentration or preservation. Fern Glen Rapids contains ~0.18 wt. % Ni in bulk (Supplementary Data 1), similar to enrichments seen in low-grade Ni ores on Earth[19]. In the Wallace Butte workspace, the average Ni in the mudstone was significantly higher, at ~0.29 wt. % (Supplementary Data 1). This includes Dragon Creek, a homogenous fine-grained target which averages ~1.1 wt. % Ni – the strongest enrichment in Ni ever seen in bedrock on Mars (Fig. 3b, Supplementary Data 1). Comparison with LIBS-derived major element composition shows that, excluding Dragon Creek (which has an unusually low Fe:Ni ratio), Ni abundance correlates with FeO_T ($R^2 = 0.66$), suggesting that Ni is primarily hosted in a Fe-bearing phase (Fig. 3a).

Context provided by PIXL Micro-XRF

PIXL (Planetary Instrument for X-Ray Lithochemistry) is an X-ray fluorescence (XRF) instrument mounted on the robotic arm of the rover[20]. With PIXL, mm-scale elemental maps are generated by irradiating rock surfaces with X-rays and measuring the characteristic fluorescence emitted as atoms relax. PIXL is capable of detecting both major and trace elements, including Ni[20]. However, precise quantification of Ni is complicated by factors including limited counting statistics, X-ray diffraction, bremsstrahlung background modeling, and the Fe K_β tailing. As a result, this study focuses on using PIXL to better understand what phases Ni is present in using elemental maps of relative abundances.

https://doi.org/10.1038/s41467-026-70081-3

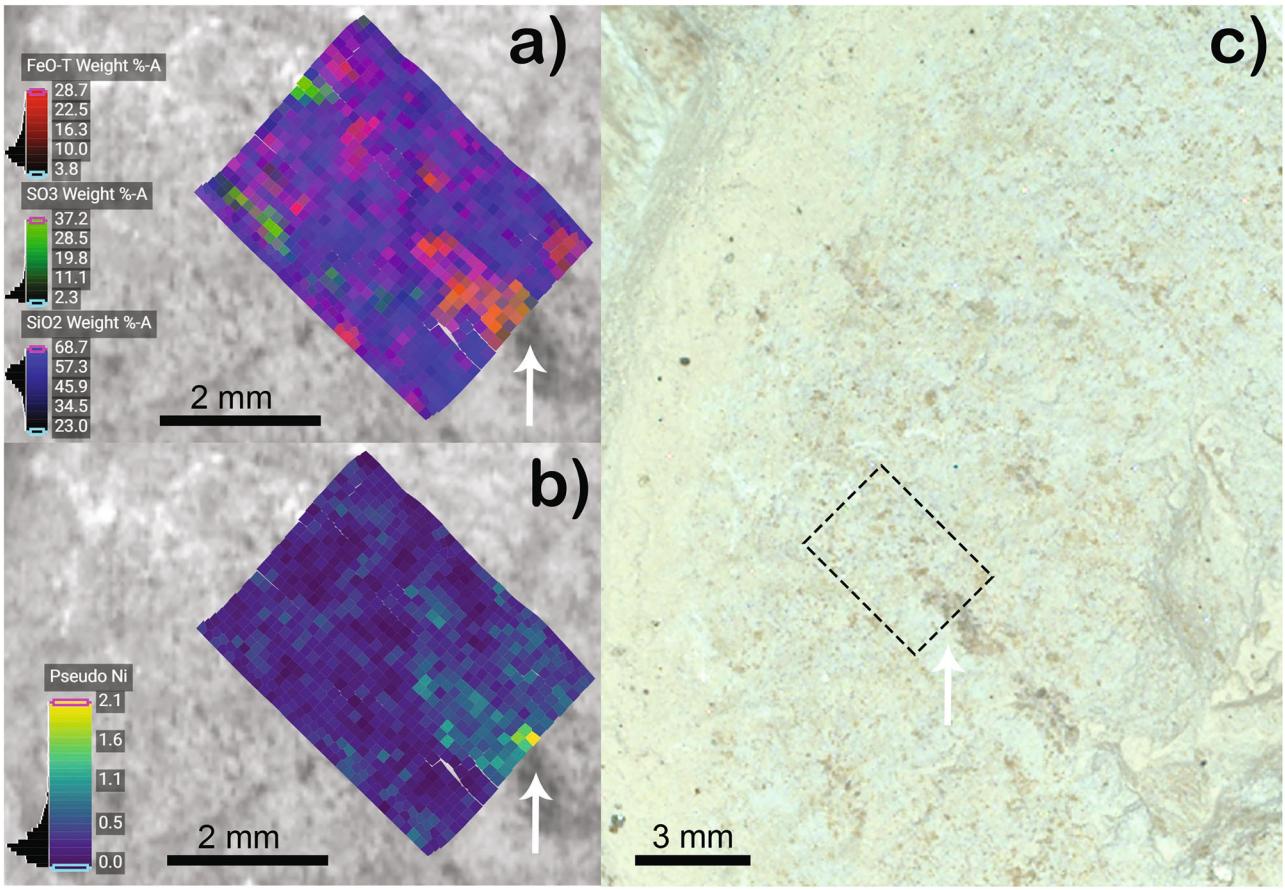

Fig. 4 | In Bright Angel mudstones, Ni is found in mm-scale, dark-toned, Fe-sulfide rich domains. PIXL micro-XRF observation from the third "Apollo Temple" scan (**a**,**b**), alongside a SHERLOC WATSON color image for context (**c**). An RGB composite shows the areas with relative enrichment of FeO_T, SO_3, and SiO_2 where brownish tones highlight Fe-sulfide (**a**). Zones of Ni enrichment are seen in yellow (**b**) and marked with white arrows (**a**,**b**,**c**). Dashed black box shows the approximate area of the PIXL scan (**c**). Image Credit: NASA/JPL-Caltech.

Across Neretva Vallis, PIXL performed 15 scans on 8 distinct rock targets. In the north of BA, PIXL explored the Beaver Falls workspace with observations of three rock targets: the Apollo Temple abrasion patch, Cheyava Falls natural surface (not inside abrasion patch), and the Steamboat Mountain abrasion patch (of the Fern Glen Rapids member). At Apollo Temple, a representative mudstone, three PIXL scans revealed Ni enrichments associated with Fe-sulfide phases. In one scan, Ni-enriched points were localized in a ~ 0.3 mm wide, dark linear vein composed of Fe-sulfide. In two other scans, Ni was concentrated in dark-toned ~1–1.5 mm domains of Fe-sulfide (Fig. 4). One of these zones has been interpreted as greigite, a metastable precursor to pyrite[7].

The Cheyava Falls natural surface, located on the same block as the Apollo Temple abrasion patch, also exhibited a ~ 1 mm Ni-rich, Fe-sulfide domain. At the Steamboat Mountain abrasion patch – stratigraphically below Apollo Temple and Cheyava Falls – PIXL identified coarse, sand- to granule-sized detrital grains of olivine and Fe-Mg carbonate surrounded by Ca-sulfate and supported in a mudstone matrix. Ni enrichments were detected primarily along the edge of olivine grains. In contrast, no enrichments in Ni were noted in either of the two PIXL scans in Southern BA and northern MT. These absences are consistent with the patterns observed by SuperCam.

PIXL observations at Wallace Butte and Malgosa Crest in southern MT revealed a different host environment for Ni. Both targets sampled the dominant mudstone lithology of this workspace. At Wallace Butte (Fig. 5b), the first scan showed Ni concentrated in a ~ 1 mm rounded, dark-toned nodule that was associated with moderate Mg and S enrichments. The second scan identified two distinct Ni-enriched zones: one ~1 mm sub-rounded Fe-Mg-S nodule and one ~0.2 mm wide linear vein rich in a phase interpreted as Mg-sulfate (Fig. 5). At Malgosa Crest, Ni was associated with irregular bright patches and small zones (~0.4–0.5 mm) of Mg-sulfate.

PIXL characterized Ni in Neretva Vallis sedimentary rocks, primarily in the form of Fe-sulfides and their sulfate alteration products, through an integrated analysis of acquired X-ray fluorescence and X-ray scatter data[21]. In the primary mudstone of Beaver Falls (Apollo Temple, Fig. 4), Ni is associated with domains of Fe-sulfide (identified by its Fe/S ratio, Fig. 6a), while stratigraphically lower conglomerates (Steamboat Mountain) exhibit Ni that is distributed adjacent to detrital olivine grains. Southward in Wallace Butte, Ni is preferentially found in irregular zones and veins of Mg-sulfate (Fig. 5b and Fig. 6b), consistent with authigenic precipitation during post-depositional alteration.

Discussion

Provenance and distribution of Ni in Neretva Vallis

Most Ni in terrestrial planets is partitioned into their metallic cores, leaving the crust highly depleted (~60 ppm on Earth)[22]. The bulk Ni concentrations presented in this study (~1.1 wt.% in Dragon Creek, for example) constitute the highest abundances ever seen in bedrock in-situ on Mars. Ni has been well documented in Martian meteorites but typically only as a minor substitution in Fe-sulfides, themselves a trace phase[23–26]. Consequently, there are few processes capable of enriching Ni to the extreme levels seen in Neretva Vallis and any such explanation must also be consistent with the bulk geochemistry and geologic context of Neretva Vallis sedimentary rocks. In particular, the observation that Ni is found concentrated in dispersed Fe-sulfides and diagenetic sulfates within Mg poor mudstones must be considered.

https://doi.org/10.1038/s41467-026-70081-3

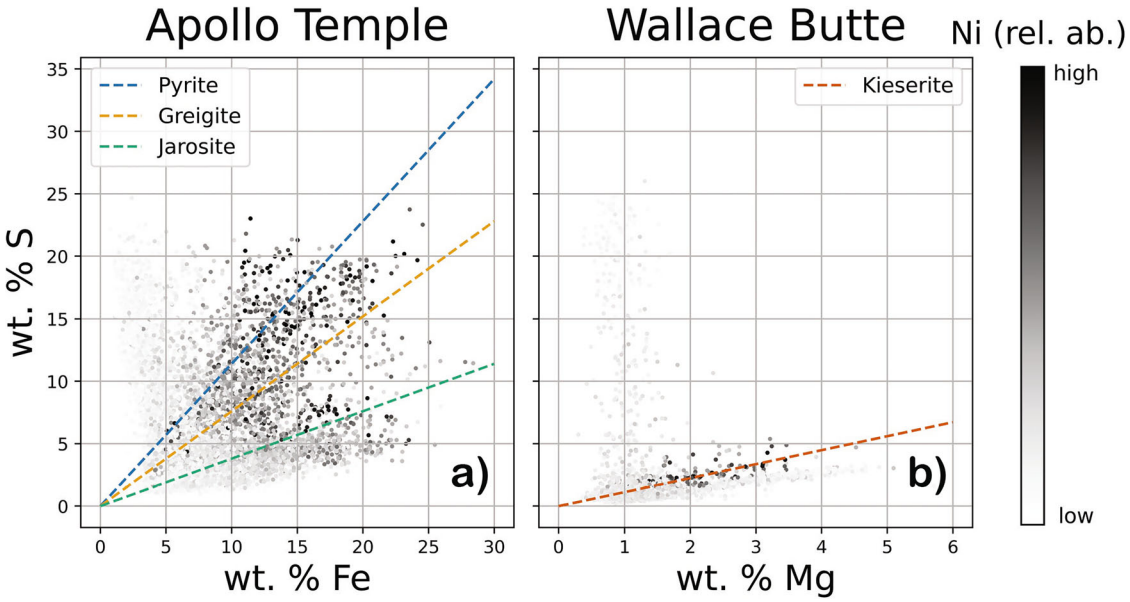

Fig. 5 | According to micro-XRF observations, Fe-sulfide and Mg-sulfate are the hosts of Ni. Scatterplots of weight percent sulfur vs iron in all three Apollo Temple PIXL scans (**a**) and weight percent sulfur vs magnesium for both Wallace Butte PIXL observations (**b**). Darker colors indicate a Ni relative abundance (RA). Mixing trends for candidate Ni host phases are shown with red shaded dashed lines; common Fe-sulfides/sulfates are shown in (**a**) and the Mg-sulfate kieserite ($MgSO_4{\cdot}H_2O$) in (**b**).

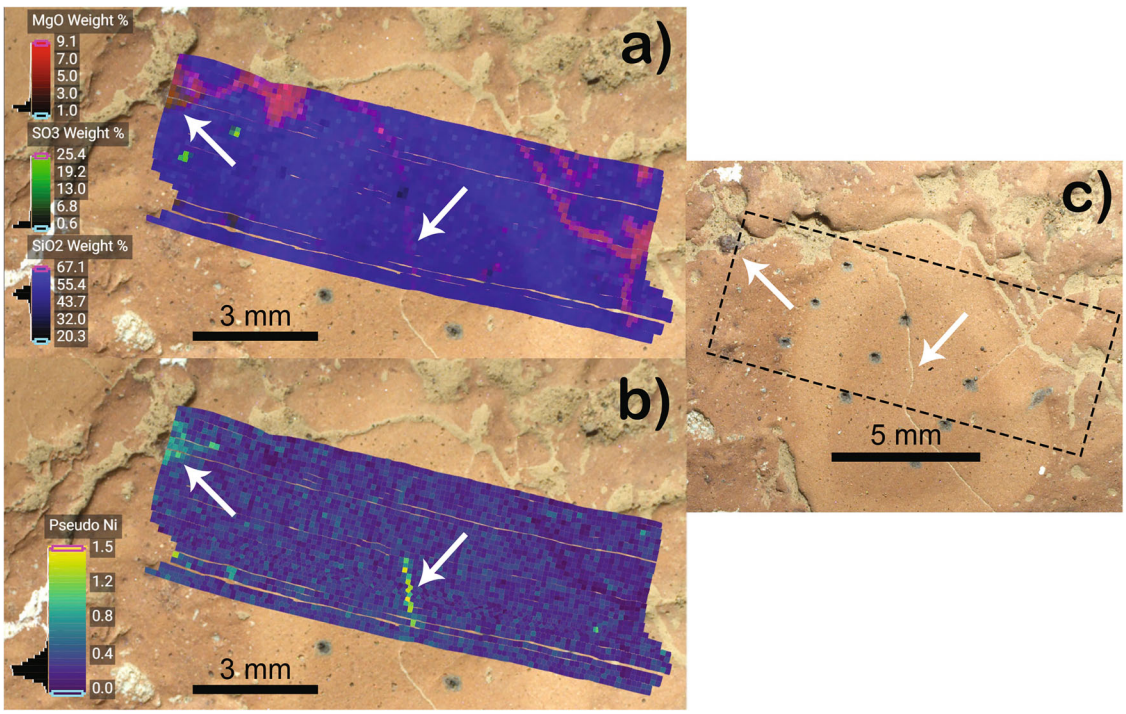

Fig. 6 | Ni is present in bright Mg-sulfate veins, supporting an authigenic origin. PIXL micro-XRF observation from the second "Wallace Butte" scan (**a**, **b**), alongside a SHERLOC WATSON color image for context (**c**). An RGB composite shows the areas with relative enrichment of MgO, SO_3, and SiO_2 where brownish tones highlight Mg-sulfate (**a**). Zones of Ni enrichment are seen in yellow (**b**) and marked with white arrows (**a**, **b**, **c**). Dashed black box shows the approximate area of the PIXL scan (**c**). Image Credit: NASA/JPL-Caltech.

There is no evidence to suggest that the Ni-rich sulfides found in Neretva Vallis were transported and deposited as grains. For example, large, rounded grains deposited in laminae or erosional scours/depressions, as is the case for terrestrial detrital pyrite are not observed[27,28]. As such, it is likely that Ni-rich material was present in the water column during or after deposition and precipitated alongside or after formation of sulfide growths in the mudstone. Although the sulfides appear authigenic in texture and morphology, the elevated Ni concentrations themselves likely reflect an influx of dissolved Ni from another source.

The original source of this Ni is, however, difficult to conclusively determine. Terrestrial komatiites and other ultramafic volcanic rocks contain ~0.2 wt. % Ni on average[22,29], with Ni typically substituting for Fe/Mg in olivine, pyroxene, and spinel. The Chassigny Martian

meteorite, which is a dunitic cumulate, contains ~500 ppm Ni, mostly in the form of nickeliferous pyrrhotite, pyrite, and pentlandite[23,26]. On Earth, when these ultramafic rocks experience prolonged and intense tropical weathering, lateritic Ni-rich soil horizons can form when Ni-bearing minerals precipitate in deep saprolite layers[30,31]. Extensive aqueous alteration results in a vertical stratification of Ni and other metals controlled by pH and Eh. In subsurface layers of terrestrial laterite, Ni can concentrate locally as high as 6 wt.%[32], mainly in Mg-bearing phyllosilicates like garnierite and nepouite[30]. Alternatively, in the upper horizons of Ni laterite, Ni is hosted in clay minerals and goethite rather than with Mg-bearing phases. Thus, in the case of Neretva Vallis mudstones, it is possible that Ni accumulations might reflect intense chemical weathering of an ultramafic protolith in the sediment source area that concentration Ni and other alteration phases within these mudstones.

Ultramafic rocks spectrally dominate the Jezero watershed and are a likely source of detrital material into Neretva Vallis[9]. The Seitah unit on Jezero crater's floor is believed to be an olivine cumulate[4], although no definitive Ni detections with SuperCam were found during Perseverance's exploration there. In northern Neretva Vallis, Ni was detected in multiple SuperCam targets several meters across the putative contact with the adjacent ultramafic Margin Unit. Shared Fe-S aqueous alteration across the Northern Margin Unit boundary with Bright Angel shows that fluids likely travelled between units. It is possible therefore that Ni became enriched through alteration of olivine in the Margin Unit and was transported into Bright Angel and precipitated in contact with pyrite and Ca-sulfate mineral veins. However, the bulk depletion of Mg observed in Neretva Vallis (~2 wt.% MgO on average) implies that ultramafic rocks and their weathering products are unlikely to be a major sediment source.

Alternatively, a meteoritic source as the ultimate origin of the Ni is a strong possibility. Debris from a Fe- and Ni-rich meteorite brought into an euxinic water column during mudstone deposition could result in the precipitation of the observed Ni-rich Fe-sulfides. However, differentiating a weathered ultramafic protolith from meteoritic Ni source would require trace metal contents (e.g., Co, Ge, Ir, Pt) and/or isotopic signatures – techniques not available to Perseverance[33].

Whatever the ultimate source of Ni, the scale, morphology, and chemistry of the observed Ni-rich Fe-sulfide domains in BA appear to resemble sedimentary pyrite (FeS_2) nodules on Earth[27,34]. During the process of pyrite nucleation and growth in terrestrial sediments, trace metals like Ni can be scavenged directly from the water column and are therefore often used to infer chemical conditions at the time of deposition[34,35]. On Earth, the Ni content of sedimentary pyrite has proven to be a key tracer of global-scale geologic processes including ocean oxidation and the emplacement of large igneous provinces[35,36]. Ni incorporated into pyrite in the Martian meteorite NWA 7533 (a regolith breccia) has been used to infer its crystallization and diagenetic conditions[24].

In terrestrial fine-grained systems, trace metal enrichment—particularly Ni—is often modulated by fluctuations in bottom-water redox conditions, sedimentation rates, and organic matter flux[37,38]. Ni commonly associates with early diagenetic pyrite in settings that oscillate between suboxic and euxinic conditions, reflecting short-lived anoxia within otherwise oxic regimes[39]. Given the spatial resolution of PIXL, sub-millimeter heterogeneity in Ni–Fe–S associations may record episodic environmental inputs such as vapor pulses or diagenetic overprinting. If so, these features could reflect transient geochemical disequilibria tied to surface–atmosphere interaction or redox boundary migration.

There is evidence for Ni mobility within Neretva Vallis sedimentary rocks. Near the contact with the adjacent Margin Unit, Ni is found in a series of Ca-rich veins interpreted as Ca-sulfate. These veins cross-cut the main mudstone lithology seen in Beaver Falls (Fig. 1). Within these veins, however, Ni appears enhanced in the most Fe-rich SuperCam observations – suggesting Ni is present in an Fe-mineral, likely a Fe-sulfate (e.g., jarosite). The field-of-view of SuperCam's infrared spectrometer is significantly larger than the LIBS spot size, which makes positive detection of Fe-sulfate within the Ca-sulfate-rich matrix difficult. The Ca-sulfate veins lack obvious oxidation halos or reaction fronts and likely postdate lithification of the mudstone, as fracturing was required for their emplacement. These relationships imply two distinct diagenetic episodes: (1) early formation of Ni-rich Fe-sulfides and (2) later precipitation of cross-cutting, Ni-bearing Ca-sulfate veins. Together, these observations suggest that Ni- and S-bearing fluids were active through multiple stages of diagenesis in Neretva Vallis.

Further south, in the Wallace Butte rock target, Ni-bearing Mg-sulfate veins are observed with PIXL (Fig. 4). Mg-Ni sulfates, largely understudied in terrestrial geologic literature, have been reported previously on Martian mudstones[40] and examined experimentally under laboratory conditions[41,42]. Within the finely laminated sediments of Gale Crater's Murray formation, the Curiosity rover found a raised diagenetic nodule which is believed to have been formed by the addition of a Mg, Ni-sulfate rich mineral[40]. The presence of Ni alongside Mg-sulfate suggests Ni^{2+} coprecipitated with or was substituted for Mg^{2+} in sulfate-rich fluids during or after mudstone deposition. Meters away from Wallace Butte, a dark high-standing rock with 0.39–0.88 wt.% Ni was discovered with an IR spectral signature and elemental chemistry consistent with jarosite ("Tower of Ra" in Fig. 1b). Within the same rover workspace is another high-standing rock with an IR spectrum resembling the chlorine-bearing Fe-oxide akaganeite. Both jarosite and akaganeite are known chemical weathering products of Fe-sulfide[43–45]. The supergene alteration of pyrrhotite ($Fe_{(1-x)}S$) to jarosite in particular has been highlighted as a likely source for gossaniferous materials found in Martian regolith[44]. Orbital and in-situ detections of akaganeite have also proven valuable in revealing local environmental conditions on early Mars[46]. Akaganeite forms in mildly acidic (~3-6), low temperature (<100 °C), and highly chlorinated aqueous environments[46]. Although most commonly found associated with hydrothermal settings, akaganeite is also an observed corrosion product of iron meteorites found in cold deserts on Earth[47].

The relationship between the Ni-rich high-standing rocks and underlying mudstone is difficult to conclusively establish. The uncertain stratigraphic relationship between the Fe-sulfide-bearing BA mudstones and the cross-channel rocks found at Wallace Butte also makes attempts at assigning any genetic relationship highly speculative. If oxygenated Cl^-- and SO_4^{2-}-bearing brines oxidized local Fe-sulfides it could explain the presence of jarosite and akaganeite – both of which require low pH conditions and would readily host Ni as a minor substitution. Alternatively, these may be exotic float rocks transported from an acid-sulfate-rich lithology somewhere in the Jezero watershed. Ni substitutions in Fe-bearing minerals are also known to significantly increase weathering resistance in meteorite samples[48]. The homogeneous and extremely high Ni content of the "Tower of Ra" target could therefore be related to its apparent erosion resistance.

Astrobiological potential of Ni-rich mudstones

On Earth, sedimentary Fe-sulfides, like those found in the Beaver Falls workspace (Fig. 1), are believed to form primarily via microbial sulfate reduction in the presence of Fe-bearing minerals[27,39]. Thermochemical reduction of sulfate is also possible at high temperatures (>150–200 °C)[39], but the BA formation shows no evidence of contact metamorphism or burial to depths associated with abiotic thermochemical sulfate reduction[7]. Furthermore, the mudstones of Neretva Vallis contain hydrated sulfate minerals and hydrated/hydroxylated clays, also pointing towards low-temperature diagenesis[7]. It is for this reason that the detection of sedimentary Fe-sulfides by PIXL, in connection with organic matter found with SHERLOC Raman

spectroscopy, has been previously described as a "potential biosignature"[7]. However, it is also possible that purely abiotic reactions, such as H_2 generation during serpentinization, contributed to the observed redox-driven organic and mineral associations. Either way, this discovery raises major questions about the potential for prebiotic or biotic chemistry on early Mars.

Ni plays a crucial role in terrestrial biology and is implicated in some of the most ancient microbial metabolisms known on Earth. In particular, Ni is an essential component of enzymes used by methanogenic archaea and many bacterial species[49–51]. Ni is vital to the metabolism of methanogenic organisms, such that a decrease in the Ni content of Earth's oceans in the Archean is hypothesized to have caused a collapse in atmospheric methane preceding the Great Oxidation Event[52]. Furthermore, the Wood-Ljungdahl (W-L) pathway, generally believed to be among the oldest known forms of energy generation and carbon fixation, requires Ni[49,53]. Parts of this pathway containing [NiFe]-hydrogenase are common between archaeal methanogens and bacterial acetogens. This suggests they were present in LUCA (the last universal common ancestor), before the split between archaea and bacteria (>4.09–4.33 Gya)[54–56]. The reverse W-L pathway, again requiring Ni, has even been observed in some species of sulfate-reducing bacteria, where it is instrumental in the decomposition organic matter[57]. The breakdown of organic matter coupled with the reduction of sulfate to sulfide is the hypothesis that has been previously raised by PIXL and SHERLOC scans in the Bright Angel formation[7].

The results of our investigation of sedimentary rocks derived from Noachian (~4.1-3.7 Gya) materials in the Jezero watershed[2,9] invite comparisons with an early Earth environment and a terrestrial biosphere that developed around the same time as these rocks. While the observations presented in this work do not necessarily imply that the distribution of Ni is related to a biological process, the presence of strong enrichments suggests it was bioavailable. As an element essential to the earliest known forms of life on Earth, and a particularly scarce trace metal, the elevated concentrations of Ni in the Beaver Falls workspace –co-located with organic matter[7] – offers an intriguing hint of past organic driven redox processes on Mars.

To more definitively resolve the source of Ni in Neretva Vallis and its possible connection with organic matter, Ni/S isotope measurements and micron-scale chemical mapping should be performed on the "Sapphire Canyon" sample collected at Beaver Falls, intended for return to Earth in a future Mars Sample Return mission.

Methods

Ni calibration with SuperCam

With SuperCam LIBS, a pulsed laser is focused on a target, typically 2–6.5 m away, generating a plasma[12,13]. The diameter of the irradiated spot ranges from 100–450 μm, increasing with distance[13]. As the plasma cools, light is emitted with a wavelength characteristic of the elements present in the sample. SuperCam collects light in three spectrometers covering the ranges 243.5–341.7 nm, 382.1–467.5 nm, and 535–853 nm[12]. Typical SuperCam operations involve taking 30 laser shots (the first 5 being used to remove dust cover) at a single location, which are then averaged[13]. The mast is then rotated to take subsequent observations in the same manner, usually completing a 10×1 raster across a rock surface[13].

Various trace elements have been detected and quantified using LIBS data from SuperCam's predecessor ChemCam, providing valuable insight into the diagenetic and aqueous history of Gale Crater[58–61]. To quantify Ni for this work, a suite of pressed powder samples was created from standards purchased from Brammer Standard Company, Inc with well characterized Ni contents. A total of 64 powder mixtures were made from several endmembers including gypsum ($CaSO_4{\cdot}2H_2O$), kaolinite ($Al_2Si_2O_5(OH)_4$), and basalt – all doped with varying amounts of Ni-oxide powder (0–22 wt. %). Samples were created by carefully weighing and thoroughly mixing the endmembers in set proportions and pressing them at 15 tons for 3 minutes using a manual hydraulic press. The samples were then shipped to Los Alamos National Laboratory, where they were analyzed by LIBS using the SuperCam Engineering Qualification Model (EQM). Samples were shot in three separate locations to account for any heterogeneity in the material. In addition to the pellets created specifically for this work, LIBS spectra collected by the SuperCam EQM from 129 samples as part of the major element calibration effort were added to the dataset to improve performance at very low (or zero) wt. % Ni. All LIBS spectra were processed via the same pipeline used for Mars data as described in Anderson et al. 2021 (dark subtraction, denoising, instrument response correction, continuum removal, etc.)[62].

Samples were then randomly divided into 5 folds, 1 for testing and 4 for training. Various multivariate regressors commonly used for LIBS elemental calibrations were implemented and compared using their root mean squared error of prediction (RMSEP) and consistency over a range of different target compositions. Partial Least Squares (PLS), Elastic Net, Support Vector Regression, Random Forest, and Extremely Randomized Trees were all attempted, each being tuned using a cross-validation technique which optimized for various hyperparameters that modify regressor performance.

Of all the regressors tested, Extremely Randomized Trees (ExtraTrees)[63] had the lowest RMSEP and most stability across target types. ExtraTrees is an ensemble machine learning method which builds a forest of binary decision trees and combines their results to make predictions[63]. ExtraTrees, and the related Random Forest algorithm, while often more challenging to interpret than traditional multivariate methods like PLS, has proven very effective in predicting both major and minor elements with SuperCam LIBS[58,62].

The ExtraTrees model developed to predict Ni with SuperCam LIBS has a RMSEP of 0.12 wt. % and the correlation coefficient (R^2) between the predicted and certified wt. % Ni in the test set is 0.9 (Fig. S2). This demonstrates that over the range of Ni tested (0–2 wt. %), the model can predict Ni content with an average error of 0.12 wt. %. In addition, the coefficients for the model can be calculated. The coefficients of an ExtraTrees model show how important each feature (spectral channel) is to the overall prediction based on its ability to split data across all decision trees. The coefficients of the chosen model are highly elevated at the Ni I emission lines at 301.288 nm, 305.170 nm, and 310.278 nm (Fig. S3). This indicates that Ni is being predicted successfully based on Ni peaks present in the training set, rather than other LIBS emission lines that are merely correlated with wt. % Ni. There are, however, other LIBS emission lines with positive loadings, meaning that virtually all SuperCam Mars data will have a predicted Ni wt. % greater than zero. The detection limit of Ni with SuperCam LIBS, based on qualitative analysis, is ~0.12 wt. % (Fig. S4) and therefore, as expected, the vast majority of SuperCam Mars spectra have no detectable Ni emission lines – this creates a number of false positives.

To prevent false positive detections of Ni in SuperCam Mars data, a line checker was implemented. Peak areas for each of the three major Ni emission lines in all SuperCam Mars data were calculated with a custom peak fitting code written in Python using the lmfit package[64]. Only Ni quantifications where all three emission lines have a peak area above a set threshold (4×10^{-5}) were reported. This ensures that false positives are eliminated. All SuperCam Mars data with Ni detections were verified to have Ni lines. A selection of the highest Ni quantifications was compared to laboratory LIBS spectra with a similar concentration of Ni to verify there was a qualitative match (e.g. Fig. S5).

PIXL XRF for qualitative analysis of Ni

PIXL (Planetary Instrument for X-Ray Lithochemistry) is a micro-X-ray fluorescence (μXRF) instrument mounted on the robotic arm of the Perseverance rover[20]. PIXL produces mm-scale elemental maps by

irradiating rock surfaces with highly focused X-rays and measuring the subsequent X-rays emitted that are diagnostic of specific electronic transitions[20]. PIXL's interrogation spot size varies with X-ray energy and has a FWHM of ~120 μm at ~8 keV[65]. Thousands of analysis spots are included in a typical PIXL map scan. Elemental quantification for each analysis spot is accomplished using PIQUANT[66], which utilizes fundamental parameters and a limited suite of calibration standards. PIXL can detect and quantify major and minor elements, as well as trace elements, including Ni[20]. Precise quantification of Ni can be complicated by several factors, including limited counting statistics, X-ray diffraction, bremsstrahlung background modeling, detector temperature, and Fe K_β tailing (e.g., VanBommel et al., 2019; 2025; Christian et al. 2023). Typical detection limits for Ni with PIXL are on the order of 100 μg/g. This study focuses on using PIXL to better understand what phases host Ni by assessing elemental maps of Ni pseudo-intensities, visualized using the PIXLISE software[20].

As discussed in Allwood et al. [20] and Lawson et al. [67], pseudo-intensities represent low data volume estimates of XRF line-intensities that are generated by the PIXL instrument onboard the *Perseverance* rover. The onboard analysis involves summing the two X-ray histograms (represented as count rates binned across 4096 detector energy channels) collected at each location in a PIXL scan. The summed histogram is then smoothed, the histogram background is estimated and subtracted, and element line intensities are estimated by integrating over channel ranges specific to elements of interest, in our case, nickel. Because the pseudo-intensity values are calculated from the sum of the signal from both of PIXL's detectors, it is possible for pseudo-intensity values to be overestimated if the measured signal from one of the two detectors contains contributions from the elastic scattering of X-rays from the PIXL X-ray source when they encounter the lattice structure of minerals in the scan area[68,69]. To ensure that our Ni-pseudo-intensity data is not affected by these diffraction phenomena, we have constructed maps of diffraction intensity in the vicinity of the Ni XRF line energy corresponding to the Ni-pseudo-intensity maps shown on Figs. 2 and 4. These diffraction intensity maps are presented in Figs. S6 and S7, and demonstrate that the pseudo-intensity of Ni shown in Figs. 4 and 5 are not the result of X-ray diffraction.

Data availability

All Perseverance (Mars 2020) rover datasets are available via the Planetary Data System (PDS), according to the Mars 2020 Data Management Plan, at this direct link: https://pds-geosciences.wustl.edu/missions/mars2020/index.htm. The LIBS spectra collected at LANL using the SuperCam EQM for the Ni calibration in this study are have been deposited in a Zenodo archive under accession code[70]: https://zenodo.org/records/15276916. The processed data of Ni abundances derived from SuperCam spectra are provided in Supplementary Data. Supplementary Data 1 is a master database with all SuperCam detections of Ni in Neretva Vallis alongside major element compositions and notes on outcrop scale observations. Supplementary Data 2 is a list of all test and training data used to create SuperCam's Ni calibration with Ni content and major element compositions. Target names correspond to. fits filenames in Zenodo archive.

References

1. Farley, K. A. et al. Mars 2020 Mission Overview. *Space Sci. Rev.* **216**, 142 (2020).
2. Fassett, C. I. & Head, J. W. The timing of martian valley network activity: Constraints from buffered crater counting. *Icarus* **195**, 61–89 (2008).
3. Horgan, B. et al. Mineralogy, Morphology, and Emplacement History of the Maaz Formation on the Jezero Crater Floor From Orbital and Rover Observations. *JGR Planets* **128**, e2022JE007612 (2023).
4. Liu, Y. et al. An olivine cumulate outcrop on the floor of Jezero crater, Mars. *Science* **377**, 1513–1519 (2022).
5. Mangold, N. et al. Perseverance rover reveals an ancient delta-lake system and flood deposits at Jezero crater, Mars. *Science* **374**, 711–717 (2021).
6. Horgan, B. H. N., Anderson, R. B., Dromart, G., Amador, E. S. & Rice, M. S. The mineral diversity of Jezero crater: Evidence for possible lacustrine carbonates on Mars. *Icarus* **339**, 113526 (2020).
7. Hurowitz, J. A. et al. Redox-driven mineral and organic associations in Jezero Crater, Mars. *Nature* **645**, 332–340 (2025).
8. Stack, K. M. et al. Photogeologic Map of the Perseverance Rover Field Site in Jezero Crater Constructed by the Mars 2020 Science Team. *Space Sci. Rev.* **216**, 127 (2020).
9. Goudge, T. A., Mustard, J. F., Head, J. W., Fassett, C. I. & Wiseman, S. M. Assessing the mineralogy of the watershed and fan deposits of the Jezero crater paleolake system, Mars. *JGR Planets* **120**, 775–808 (2015).
10. Brown, A. J., Viviano, C. E. & Goudge, T. A. Olivine-Carbonate Mineralogy of the Jezero Crater Region. *JGR Planets* **125**, e2019JE006011 (2020).
11. Royer, C. et al. Intense alteration on early Mars revealed by high-aluminum rocks at Jezero crater. *Commun. Earth Environ.* **5**, 671 (2024).
12. Wiens, R. C. et al. The SuperCam Instrument Suite on the NASA Mars 2020 Rover: Body Unit and Combined System Tests. *Space Sci. Rev.* **217**, 4 (2021).
13. Maurice, S. et al. The SuperCam Instrument Suite on the Mars 2020 Rover: Science Objectives and Mast-Unit Description. *Space Sci. Rev.* **217**, 47 (2021).
14. Rivera-Hernández, F. et al. Grain Size Variations in the Murray Formation: Stratigraphic Evidence for Changing Depositional Environments in Gale Crater, Mars. *JGR Planets* **125**, e2019JE006230 (2020).
15. Kramida, A. & Ralchenko, Y. NIST Atomic Spectra Database, NIST Standard Reference Database 78. National Institute of Standards and Technology https://doi.org/10.18434/T4W30F (1999).
16. Dehouck, E., Mandon, L., Johnson, J., Manelski, H. T. & Wolf, U. Iron-rich, Akaganeite- and Jarosite-bearing Rocks on the Flank of Neretva Vallis, Jezero Crater. 56th Lunar and Planetary Science Conference, 2760 (2025).
17. Bishop, J. L. & Murad, E. The visible and infrared spectral properties of jarosite and alunite. *Am. Mineralogist* **90**, 1100–1107 (2005).
18. Bishop, J. L., Murad, E. & Dyar, M. D. Akaganeite and schwertmannite: Spectral properties and geochemical implications of their possible presence on Mars. *Am. Mineralogist* **100**, 738–746 (2015).
19. Bide, T., Hetherington, L. & Gunn, G. Nickel. (2008).
20. Allwood, A. C. et al. PIXL: Planetary Instrument for X-Ray Lithochemistry. *Space Sci. Rev.* **216**, 134 (2020).
21. Dehouck, E. et al. Evaluating the role of sulfide-weathering in the formation of sulfates or carbonates on Mars. *Geochimica et. Cosmochimica Acta* **90**, 47–63 (2012).
22. Yaroshevsky, A. A. Abundances of chemical elements in the Earth's crust. *Geochem. Int.* **44**, 48–55 (2006).
23. Lorand, J.-P. et al. Petrogenesis of martian sulfides in the Chassigny meteorite. *Am. Mineralogist* **103**, 872–885 (2018).
24. Lorand, J. et al. Nickeliferous pyrite tracks pervasive hydrothermal alteration in Martian regolith breccia: A study in NWA 7533. *Meteorit. Planet. Scien* **50**, 2099–2120 (2015).
25. Lorand, J.-P., Chevrier, V. & Sautter, V. Sulfide mineralogy and redox conditions in some shergottites. *Meteorit. Planet. Sci.* **40**, 1257–1272 (2005).
26. Lodders, K. A survey of shergottite, nakhlite and chassigny meteorites whole-rock compositions. *Meteorit & Planetary Scien* **33**, A183–A190 (1998).
27. Rickard, D. Sedimentary Pyrite. in *Developments in Sedimentology* vol. **65**, 233–285 (Elsevier, 2012).

28. Da Costa, G., Hofmann, A. & Agangi, A. Provenance of Detrital Pyrite in Archean Sedimentary Rocks. in *Sediment Provenance* 509–531 (Elsevier, 2017). https://doi.org/10.1016/B978-0-12-803386-9.00018-6.
29. Barnes, S. J. & Brand, N. W. The distribution Cr, Ni, and chromite in komatiites, and application to exploration for komatiite-hosted nickel sulfide deposits. *Economic Geol.* **94**, 129–132 (1999).
30. Butt, C. R. M. & Cluzel, D. Nickel Laterite Ore Deposits: Weathered Serpentinites. *Elements* **9**, 123–128 (2013).
31. Gleeson, S. A., Butt, C. R. M. & Elias, M. Nickel Laterites: A Review. *SEG Discovery* 1–18 (2003) https://doi.org/10.5382/SEGnews.2003-54.fea.
32. Gleeson, S. A., Herrington, R. J., Durango, J., Velasquez, C. A. & Koll, G. The Mineralogy and Geochemistry of the Cerro Matoso S.A. Ni Laterite Deposit, Montelibano, Colombia. *Economic Geol.* **99**, 1197–1213 (2004).
33. Koglin, N., Frimmel, H. E., Lawrie Minter, W. E. & Brätz, H. Trace-element characteristics of different pyrite types in Mesoarchaean to Palaeoproterozoic placer deposits. *Min. Depos.* **45**, 259–280 (2010).
34. Gregory, D. et al. The formation mechanisms of sedimentary pyrite nodules determined by trace element and sulfur isotope microanalysis. *Geochimica et. Cosmochimica Acta* **259**, 53–68 (2019).
35. Large, R. R. et al. Trace element content of sedimentary pyrite as a new proxy for deep-time ocean–atmosphere evolution. *Earth Planet. Sci. Lett.* **389**, 209–220 (2014).
36. Mukherjee, I. & Large, R. R. Co-evolution of trace elements and life in Precambrian oceans: The pyrite edition. *Geology* **48**, 1018–1022 (2020).
37. Tribovillard, N., Algeo, T. J., Lyons, T. & Riboulleau, A. Trace metals as paleoredox and paleoproductivity proxies: An update. *Chem. Geol.* **232**, 12–32 (2006).
38. Raiswell, R. & Canfield, D. E. Sources of iron for pyrite formation in marine sediments. *Am. J. Sci.* **298**, 219–245 (1998).
39. Machel, H. G. Bacterial and thermochemical sulfate reduction in diagenetic settings — old and new insights. *Sediment. Geol.* **140**, 143–175 (2001).
40. VanBommel, S. J. et al. Deconvolution of distinct lithology chemistry through oversampling with the Mars Science Laboratory Alpha Particle X-Ray Spectrometer. *X-Ray Spectrom.* **45**, 155–161 (2016).
41. Talla, D., Balla, M., Aicher, C., Lengauer, C. L. & Wildner, M. Structural and spectroscopic study of the kieserite-dwornikite solid-solution series, (Mg,Ni)SO4·H2O, at ambient and low temperatures, with cosmochemical implications for icy moons and Mars. *Am. Mineralogist* **105**, 1472–1489 (2020).
42. Talla, D., Giester, G. & Wildner, M. Structural and spectroscopic study of the kieserite-type (Mg,Mn)SO4·H2O solid solution at ambient and low temperatures relevant to Mars and the icy moons of Jupiter and Saturn. *Icarus* **401**, 115583 (2023).
43. Burns, R. G. Rates and mechanisms of chemical weathering of ferromagnesian silicate minerals on Mars. *Geochimica et. Cosmochimica Acta* **57**, 4555–4574 (1993).
44. Burns, R. G. & Fisher, D. S. Iron-sulfur mineralogy of Mars: Magmatic evolution and chemical weathering products. *J. Geophys. Res.* **95**, 14415–14421 (1990).
45. Elwood Madden, M. E., Bodnar, R. J. & Rimstidt, J. D. Jarosite as an indicator of water-limited chemical weathering on Mars. *Nature* **431**, 821–823 (2004).
46. Carter, J., Viviano-Beck, C., Loizeau, D., Bishop, J. & Le Deit, L. Orbital detection and implications of akaganéite on Mars. *Icarus* **253**, 296–310 (2015).
47. Buchwald, V. F. & Clarke, R. S. Jr Akaganeite, not Lawrencite, Corrodes Antarctic Iron Meteorites. *Meteoritics* **23**, 261 (1988).
48. Lee, M. R. & Bland, P. A. Mechanisms of weathering of meteorites recovered from hot and cold deserts and the formation of phyllosilicates. *Geochimica et. Cosmochimica Acta* **68**, 893–916 (2004).
49. Fontecilla-Camps, J. C. Nickel and the origin and early evolution of life. *Metallomics* **14**, mfac016 (2022).
50. Zhang, Y. & Gladyshev, V. N. General Trends in Trace Element Utilization Revealed by Comparative Genomic Analyses of Co, Cu, Mo, Ni, and Se. *J. Biol. Chem.* **285**, 3393–3405 (2010).
51. Scherer, P., Lippert, H. & Wolff, G. Composition of the major elements and trace elements of 10 methanogenic bacteria determined by inductively coupled plasma emission spectrometry. *Biol. Trace Elem. Res* **5**, 149–163 (1983).
52. Konhauser, K. O. et al. Oceanic nickel depletion and a methanogen famine before the Great Oxidation Event. *Nature* **458**, 750–753 (2009).
53. Russell, M. J. & Martin, W. The rocky roots of the acetyl-CoA pathway. *Trends Biochemical Sci.* **29**, 358–363 (2004).
54. Borrel, G., Adam, P. S. & Gribaldo, S. Methanogenesis and the Wood–Ljungdahl Pathway: An Ancient, Versatile, and Fragile Association. *Genome Biol. Evol.* **8**, 1706–1711 (2016).
55. Betts, H. C. et al. Integrated genomic and fossil evidence illuminates life's early evolution and eukaryote origin. *Nat. Ecol. Evol.* **2**, 1556–1562 (2018).
56. Moody, E. R. R. et al. The nature of the last universal common ancestor and its impact on the early Earth system. *Nat. Ecol. Evol.* **8**, 1654–1666 (2024).
57. Spormann, A. M. & Thauer, R. K. Anaerobic acetate oxidation to CO2 by Desulfotomaculum acetoxidans: Demonstration of enzymes required for the operation of an oxidative acetyl-CoA/carbon monoxide dehydrogenase pathway. *Arch. Microbiol.* **150**, 374–380 (1988).
58. Gasda, P. J. et al. Quantification of manganese for ChemCam Mars and laboratory spectra using a multivariate model. *Spectrochimica Acta Part B: At. Spectrosc.* **181**, 106223 (2021).
59. Ollila, A. M. et al. Trace element geochemistry (Li, Ba, Sr, and Rb) using *Curiosity*'s ChemCam: Early results for Gale crater from Bradbury Landing Site to Rocknest. *JGR Planets* **119**, 255–285 (2014).
60. Payré, V. et al. Copper enrichments in the Kimberley formation in Gale crater, Mars: Evidence for a Cu deposit at the source. *Icarus* **321**, 736–751 (2019).
61. Goetz, W. et al. Detection of Copper by the ChemCam Instrument Along Curiosity's Traverse in Gale Crater, Mars: Elevated Abundances in Glen Torridon. *JGR Planets* **128**, e2021JE007101 (2023).
62. Anderson, R. B. et al. Post-landing major element quantification using SuperCam laser induced breakdown spectroscopy. *Spectrochimica Acta Part B: At. Spectrosc.* **188**, 106347 (2022).
63. Geurts, P., Ernst, D. & Wehenkel, L. Extremely randomized trees. *Mach. Learn* **63**, 3–42 (2006).
64. Newville, M., Stensitzki, T., Allen, D. B. & Ingargiola, A. LMFIT: Non-Linear Least-Square Minimization and Curve-Fitting for Python. Zenodo https://doi.org/10.5281/ZENODO.11813 (2014).
65. Das, A. et al. Energy dependence of x-ray beam size produced by polycapillary x-ray optics. *X-Ray Spectrom.* **54**, 203–213 (2025).
66. Heirwegh, C. M., Elam, W. T., O'Neil, L. P., Sinclair, K. P. & Das, A. The focused beam X-ray fluorescence elemental quantification software package PIQUANT. *Spectrochimica Acta Part B: At. Spectrosc.* **196**, 106520 (2022).
67. Lawson, P. R. et al. Adaptive sampling with PIXL on the Mars Perseverance rover. *Icarus* **429**, 116433 (2025).
68. Tice, M. M. et al. Alteration history of Séítah formation rocks inferred by PIXL x-ray fluorescence, x-ray diffraction, and multispectral imaging on Mars. *Sci. Adv.* **8**, 47 (2022).
69. Jones, M. W. M. et al. In situ crystallographic mapping constrains sulfate precipitation and timing in Jezero crater, Mars. *Sci. Adv.* **11**, 16 (2025).
70. Manelski, H. SuperCam Ni Calibration and Mars Data. Zenodo https://doi.org/10.5281/ZENODO.15276915 (2025).

Acknowledgements
This work was supported in the United States by the NASA Mars Exploration Program (grant number NNH13ZDA018O for H.T.M., R.C.W., S.A.C., and S.C.) and LANL and in France by CNES and CNRS. Support in Germany was provided by DLR. Composition and spectra of Ni-rich sulfates were provided by the Centre for Terrestrial and Planetary Exploration (C-TAPE) at the University of Winnipeg (http://www.uwinnipeg.ca/c-tape). Any use of trade, firm, or product names is for descriptive purposes only and does not imply endorsement by the U.S. Government.

Author contributions
H.T.M. and R.C.W. conceptualized the study. H.T.M. prepared the sample suite and performed the multivariate Ni calibration. S.C. and R.K.M. analyzed the Ni calibration samples with the SuperCam EQM at LANL. H.T.M., A.B., J.A.H., M.T., E.D., C.C.B., E.A.C., A.C., S.J.V., E.D., N.R., S.A.C., T.S.J.G., S.S., O.F., L.M., and M.L.C. contributed to the methodology and analyses of SuperCam and PIXL data. H.T.M. prepared the manuscript. All co-authors reviewed and commented on the manuscript.

Competing interests
The authors declare no competing interests.

Additional information
Supplementary information The online version contains supplementary material available at https://doi.org/10.1038/s41467-026-70081-3.

Correspondence and requests for materials should be addressed to H. T. Manelski.

Peer review information *Nature Communications* thanks Janice Bishop and the other, anonymous, reviewer(s) for their contribution to the peer review of this work. A peer review file is available.